# QGSM Predictions for Net-Baryon Production in Nucleus-Nucleus Collisions

G.H. Arakelyan[1], C. Merino[2], Yu.M. Shabelski[3]

*1.A.Alikhanyan National Scientific Laboratory*
*(Yerevan Physics Institute)*
*Yerevan, Armenia*
*2.Departamento de Física de Partículas*
*Instituto Galego de Física de Altas Enerxías (IGFAE)*
*Universidade de Santiago de Compostela*
*Galiza, Spain*
*3.Petersburg Nuclear Physics Institute*
*NCR Kurchatov Institute*
*Gatchina, St.Petersburg, Russia*

**International Moscow Phenomenology Workshop**
**devoted to the memory of Prof. Alexei B. Kaidalov**

*July* $21^{st}$-$25^{th}$, 2013

## Main Aim:

The Quark Gluon String Model (QGSM) predictions for net proton and net $\Lambda$-hyperon spectra, as well as for the inclusive densities of $\Lambda$ and $\bar{\Lambda}$ are compared to the experimental data.

The contributions of String Junction diffusion, interactions with nuclear clusters, and the inelastic screening corrections are accounted for.

The predictions for LHC energies are also presented

**G.H. Arakelyan, C. Merino, and Yu.M. Shabelski,**
**arXiv:1305.0388[hep-ph]**

The Quark-Gluon String Model (QGSM) is based on the Dual Topological Unitarization, Regge phenomenology, and non-perturbative QCD.

**A.B. Kaidalov and K.A. Ter-Martirosyan, Yad. Fiz. 39, 1545 (1984); 40, 211 (1984)**

The QGSM is successfully used for the description of multiparticle production processes in hadron-hadron, hadron-nucleus, and nucleus-nucleus collisions.

**A.B Kaidalov and O.I. Piskounova, Yad. Fiz. 41, 1278 (1985), Z. Phys. C30, 145 (1986)**

**G.H. Arakelyan, C. Merino, C. Pajares, and Yu.M. Shabelski, Eur. Phys. J. C54, 577 (2008) and hep-ph/0709.3174**

**A.B. Kaidalov, K.A. Ter-Martirosyan, and Yu.M. Shabelski, Yad. Fiz. 43, 1282 (1986)**

**Yu.M. Shabelski, Yad. Fiz. 50, 239 (1989)**

In this work we consider the yields of $p$ and $\bar{p}$, as well as $\Lambda$ and $\bar{\Lambda}$, produced in the collisions of different nuclei at CERN SpS and RHIC energies.

In QCD hadrons are composite bound state configurations built up from the quark and gluon fields.

In the QGSM high energy interactions are considered as proceeding via the exchange of one or several Pomerons, and all elastic and inelastic processes result from cutting through or between Pomerons.
**V.A. Abramovsky, V.N. Gribov, and O.V. Kancheli, Yad. Fiz. 18, 595 (1973)**

Inclusive spectra of hadrons are related to the corresponding fragmentation functions of quarks and diquarks, which are constructed using the Reggeon counting rules
**A.B. Kaidalov, Sov. J. Nucl. Phys. 45, 902 (1987); Yad. Fiz. 43, 1282 (1986)**

In the case of interaction with nuclear target, the Multiple Scattering Theory (Gribov-Glauber Theory) allows to consider the interaction with nucleus as the superposition of interactions with different numbers of target nucleons.

In the case of nucleus-nucleus collisions the Multiple Scattering Theory allows also to consider the interaction as the superposition of separate nucleon-nucleon interactions.

Though the analytical summation of all the diagrams is impossible, the significant classes of diagrams can be analytically summed up in the so-called rigid target approximation.
**G.D. Alkhazov et al., Nucl. Phys. A280, 365 (1977)**

In QGSM the significant differences in the yields of baryons and antibaryons in the central (midrapidity) region present even at high energies can be explained by SJ diffusion.
**F. Bopp and Yu.M. Shabelski, Yad. Fiz. 68, 2155 (2005) and hep-ph/0406158; Eur. Phys. J. A28, 237 (2006) and hep-ph/0603193**
**O.I. Piskounova, Phys. Atom. Nucl. 70, 1110 (2007) and hep-ph/0604157**

One additional contribution comes from the coherent interaction of a projectile with multiquark clusters inside the nuclei (cumulative effect). **L.L. Frankfurt and M.I. Strikman, Phys. Rep. 76, 215 (1981)**

The incorporation of these cumulative contributions into the frame of the QGSM allows the theoretical description of a number of experimental facts.
**A.V. Efremov, A.B. Kaidalov, G.I. Lykasov, and N.V. Slavin, Phys. Atom. Nucl. 57, 874 (1994)**

# General Approach

In QGSM, each exchanged Pomeron corresponds to a cylindrical diagram.

When cutting one Pomeron, two showers of secondaries are produced.

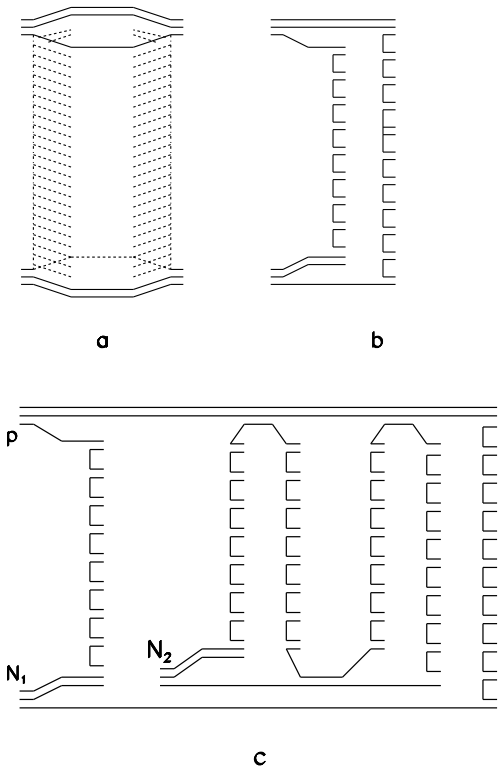


Figure 1: (a) Cylindrical diagram representing a Pomeron exchange within the DTU classification (quarks are shown by solid lines); (b) One cut of the cylindrical diagram corresponding to the single-Pomeron exchange contribution in inelastic $pp$ scattering; (c) One of the diagrams for the inelastic interaction of one incident proton with two target nucleons $N_1$ and $N_2$ in a $pA$ collision.

The inclusive spectrum of a secondary hadron $h$ results of the convolution of the diquark, valence quark, and sea quark distributions, $u(x,n)$, in the incident particles, with the fragmentation functions, $G^h(z)$, of quarks and diquarks into the secondary hadron $h$.

Both the distributions and the fragmentation functions are constructed using the Reggeon counting rules.

In particular, in the case of $n > 1$, i.e. in the case of multipomeron exchange, the distributions of valence quarks and diquarks are softened due to the appearance of a sea quark contribution.

There is some freedom in how to account for this effect.
**A.B. Kaidalov, K.A. Ter-Martirosyan, and Yu.M. Shabelski, Yad. Fiz. 43, 1282 (1986)**

In principle, the valence and sea quarks can depend on $n$ in a different manner, for example:

$$\begin{aligned}
u_{uu}(x,n) &= C_{uu}\cdot x^{\alpha_R-2\alpha_B+1}\cdot(1-x)^{-\alpha_R+m_1} \\
u_{ud}(x,n) &= C_{ud}\cdot x^{\alpha_R-2\alpha_B}\cdot(1-x)^{-\alpha_R+m_2} \\
u_{u}(x,n) &= C_{u}\cdot x^{-\alpha_R}\cdot(1-x)^{\alpha_R-2\alpha_B+m_2} \\
u_{d}(x,n) &= C_{d}\cdot x^{-\alpha_R}\cdot(1-x)^{\alpha_R-2\alpha_B+1+m_1} \\
u_{s}(x,n) &= C_{d}\cdot x^{-\alpha_R}\cdot(1-x)^{\alpha_R-2\alpha_B+(n-1)+d} \,,
\end{aligned}$$

where every distribution $u_i(x,n)$ is normalized to unity, $d$ is a parameter, and the values of $m_1$ and $m_2$ can be found from the conditions:

$$\begin{aligned}
\langle x_{uu}\rangle + \langle x_d\rangle + 2(n-1)\cdot\langle x_s\rangle &= 1 \\
\langle x_{ud}\rangle + \langle x_u\rangle + 2(n-1)\cdot\langle x_s\rangle &= 1 \,.
\end{aligned}$$

The details of the model have been presented in

**A.B. Kaidalov and K.A. Ter-Martirosyan, Yad. Fiz. 39, 1545 (1984); 40, 211 (1984)**
**A.B. Kaidalov and O.I. Piskounova, Yad. Fiz. 41, 1278 (1985); Z. Phys. C30, 145 (1986)**
**Yu.M. Shabelski, Yad. Fiz. 44, 186 (1986)**
**G.H. Arakelyan, A. Capella, A.B. Kaidalov, and Yu.M. Shabelski, Eur. Phys. J. C26, 81 (2002) and hep-ph/0103337**

The averaged number of exchanged Pomerons $\langle n \rangle_{pp}$ slowly increases with the energy.

# Inclusive Spectra of Secondary Hadrons in the QGSM

The inclusive spectra of a secondary hadron $h$ is determined in QGSM by the expression

$$\frac{dn}{dy} = \frac{x_E}{\sigma_{inel}} \cdot \frac{d\sigma}{dx_F} = \sum_{n=1}^{\infty} w_n \cdot \phi_n^h(x_F) + w_D \cdot \phi_D^h(x)$$

where $x_E = E/E_{max}$, $w_n = \sigma_n / \sum_{n=1}^{\infty} \sigma_n$ the weight of the diagram with $n$ cut Pomerons, and the term $w_D \cdot \phi_D^h(x)$ accounts for the contribution of diffraction dissociation processes.

The function $\phi_n^h(x_F)$ determines the contribution of the diagram in which $n$ Pomerons are cut. In the case of $pp$ collisions this function has the form:

$$\begin{aligned}\phi_n^{pp\to h}(x_F) = f_{qq}^h(x_+,n)\cdot f_q^h(x_-,n)\\ +f_q^h(x_+,n)\cdot f_{qq}^h(x_-,n)\\ +2(n-1)f_s^h(x_+,n)\cdot f_s^h(x_-,n)\ ,\end{aligned}$$

with

$$x_\pm = \frac{1}{2}\left[\left(\frac{4m_\perp^2}{s}+x_F^2\right)^{\frac{1}{2}} \pm x_F\right]\ ,$$

where $f_{qq}$, $f_q$, and $f_s$ correspond to the contributions of diquarks, valence quarks, and sea quarks, respectively.

The contributions of the incident particle and the target proton depend on the variables $x_+$ and $x_-$, respectively, and they are determined by the convolution of the diquark and quark distributions with the fragmentation functions, e.g.,

$$f_q^h(x_+, n) = \int_{x_+}^1 u_q(x_1, n) \cdot G_q^h(x_+/x_1) dx_1.$$

The diquark and quark distributions, as well as the fragmentation functions, are determined through Regge intercepts.

In the calculation of the inclusive spectra of secondaries produced in $pA$ collisions we should consider the possibility of one or several Pomeron cuts in each of the $\nu$ blobs of proton-nucleon inelastic interactions.

For example, the contribution of the diagram in Fig. 1c to the inclusive spectrum is

$$\begin{aligned}
\frac{x_E}{\sigma_{prod}^{pA}} \cdot \frac{d\sigma}{dx_F} &= 2 \cdot W_{pA}(2) \cdot w_1^{pN_1} \cdot w_2^{pN_2} \\
&\cdot \left\{ f_{qq}^h(x_+, 3) \cdot f_q^h(x_-, 1) \right. \\
&+ f_q^h(x_+, 3) \cdot f_{qq}^h(x_-, 1) \\
&+ f_s^h(x_+, 3) \cdot [f_{qq}^h(x_-, 2) + f_q^h(x_-, 2) \\
&+ \left. 2 \cdot f_s^h(x_-, 2)] \right\} \ ,
\end{aligned}$$

where $W_{pA}(2)$ is the probability of interaction with namely two target nucleons.

It is essential to take into account all digrams with every possible Pomeron configuration and its corresponding permutations.

The diquark and quark distributions and the fragmentation functions are the same as in the case of $pN$ interaction.

The total number of exchanged Pomerons becomes as large as

$$\langle n \rangle_{pA} \sim \langle \nu \rangle_{pA} \cdot \langle n \rangle_{pN} \ ,$$

where $\langle \nu \rangle_{pA}$ is the average number of inelastic collisions inside the nucleus (about 4 for heavy nuclei at SpS energies).

The process shown in Fig. 1c satisfies the condition that the absorptive parts of the hadron-nucleus amplitude are determined by the combination of the absorptive parts of the hadron-nucleon amplitudes.

In the case of a nucleus-nucleus collision:

1. In the fragmentation region of projectile we consider that the beam of independent nucleons of the projectile interact with the target nucleus, what corresponds to the rigid target approximation of Glauber Theory.

2. In the target fragmentation region, on the contrary, the beam of independent target nucleons interact with the projectile nucleus.

1. and 2. coincide in the central region.

The corrections for energy conservation play here a very important role if the initial energy is not very high.

This approach was used in for the successful description of $\pi^{\pm}$, $K^{\pm}$, $p$, and $\bar{p}$ produced in Pb-Pb collisions at 158 GeV per nucleon.

**J. Dias de Deus and Yu.M. Shabelski, Yad. Fiz. 71, 191 (2008)**

In QCD hadrons are composite bound state configurations built up from the quark and gluon fields.

In the string models the baryon wave function can be defined as a Star-$Y$ configuration (Fig. 2) of the gluon field, called String Junction (SJ).

**X. Artru, Nucl. Phys. B85, 442 (1975)**
**G.C. Rossi and G. Veneziano, Nucl. Phys. B123, 507 (1977)**

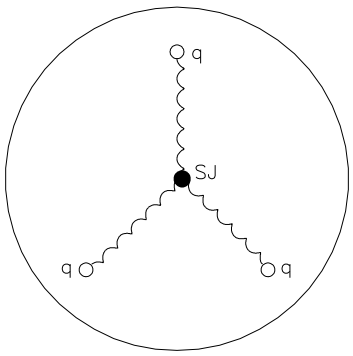


Figure 2: Composite structure of a baryon in string models.

In the case of inclusive reactions the baryon number transfer to large rapidity distances in nucleon-nucleon reactions can be explained by SJ diffusion.

# Baryon/Antibaryon Asymmetry in the QGSM

We consider the spectra of secondary baryons and antibaryons, as well as their differences, i.e. the net baryon spectra.

In the processes with incident baryons a new possibility to produce a secondary baryon in the central region exists, called SJ diffusion.

Quantitative description of the baryon number transfer due to SJ diffusion in rapidity space in
**G.H. Arakelyan, A. Capella, A.B. Kaidalov, and Yu.M. Shabelski, Eur. Phys. J. C26, 81 (2002) and hep-ph/0103337**
**O.I. Piskounova, Phys. Atom. Nucl. 70, 1110 (2007) and hep-ph/0604157**

In the QGSM the differences in the spectra of secondary baryons and antibaryons appear for processes which present SJ diffusion in rapidity space.

These differences only vanish rather slowly when the energy increases.

# String Junction Contribution

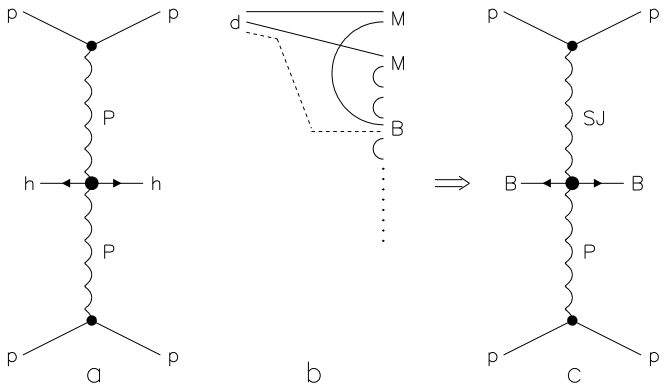


Figure 3: (a) One-Pomeron-pole diagram determining secondary hadron $h$ production. (b) String Junction (shown by dashed line) diffusion that leads to asymmetry in baryon/antibaryon production in the central region, and (c) the Reggeon diagram which describes this process.

The diagram in Fig. 3a predicts equal inclusive yields for each particle and its antiparticle, but some corrections to the spectra of secondary baryons appear in rapidity space for processes which present SJ diffusion (Fig. 3c).

The production of a baryon-antibaryon pair in the central region usually occurs via $SJ$-$\overline{SJ}$ pair production (SJ has upper color indices, whereas anti-SJ ($\overline{SJ}$) has lower indices), which then combines with sea quarks and sea antiquarks into a $B\bar{B}$ pair.

To obtain the net baryon charge, we consider three different possibilities:

1. The fragmentation of the diquark giving rise to a leading baryon (Fig. 4b).

2. The production of a leading meson in the first break-up of the string and a baryon in a subsequent break-up (Fig. 4c).

3. Both initial valence quarks recombine with sea antiquarks into mesons, $M$, while a secondary baryon is formed by the SJ together with three sea quarks (Fig. 4d).

In the two first cases the baryon number transfer is possible only for short distances in rapidity.

Figure 4: QGSM diagrams describing secondary baryon production: (a) usual $B\bar{B}$ central production with production of new SJ pair; (b) initial SJ together with two valence quarks and one sea quark; (c) initial SJ together with one valence quark and two sea quarks; (d) initial SJ together with three sea quarks.

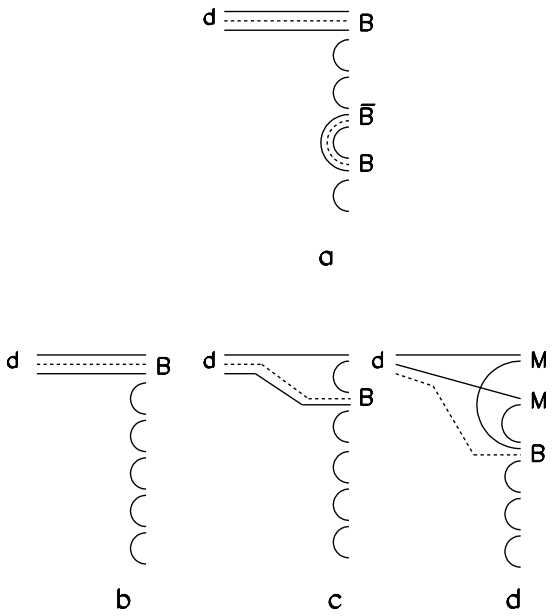


Fragmentation Functs. $\Downarrow$ $\Downarrow$ $\Downarrow$

$$G \sim \left[v_{qq}\cdot(a) + v_q\cdot(b) + v_0\cdot(c)\right]\cdot z^{\beta}$$

$$(b)\ G^B_{qq}(z) = a_N\cdot v^B_{qq}\cdot z^{2.5}\ ,$$

$$(c)\ G^B_{qs}(z) = a_N\cdot v^B_{qs}\cdot z^2(1-z)\ ,$$

$$(d)\ G^B_{ss}(z) = a_N\cdot\varepsilon\cdot v^B_{ss}\cdot z^{1-\alpha_{SJ}}(1-z)^2\ .$$

The coefficient $a_N$ is the normalization parameter, and $v_{qq}^B$, $v_{qs}^B$, $v_{ss}^B$ are the relative probabilities for different baryons production that can be found by simple quark combinatorics.

These probabilities depend on the strangeness suppression factor $S/L$, and we use $S/L = 0.32$ in the following.

The contribution of the graph in Fig. 4d has a coefficient $\varepsilon$ which determines the small probability of such baryon number transfer.

The fraction of the incident baryon energy carried by the secondary baryon decreases from (b) to (d), whereas the mean rapidity gap between the incident and secondary baryon increases.

Only the processes in Fig. 4d can contribute to the inclusive spectra in the central region at high energies if the value of the intercept of the SJ exchange Regge-trajectory, $\alpha_{SJ}$, is large enough.

The analysis gives a value of $\alpha_{SJ} = 0.5 \pm 0.1$, that is in agreement with the ALICE Collaboration result, $\alpha_{SJ} \sim 0.5$, obtained at LHC.

**C. Merino, M.M. Ryzhinski, and Yu.M. Shabelski, Eur. Phys. J. C62, 491 (2009)**

**K. Aamodt et al., ALICE Collaboration, Phys. Rev. Lett. 105, 072002 (2010) and arXiv:1006.5432[hep-ex]**

In the calculations of these effects we use the following values of the parameters:

$$\alpha_{SJ} = 0.5 \ \text{ and } \varepsilon = 0.0757\,.$$

# Contribution from Interactions with Clusters

In the case of interaction with a nuclear target some secondaries can be produced in the kinematical region forbidden for the interaction with a free nucleon (Cumulative Processes).

Usually, the cumulatie processes are considered as a result of the coherent interaction of a projectile with a multiquark cluster, i.e. with a group of several nucleons which are at short distances from each other.

**L.L. Frankfurt and M.I. Strikman, Phys. Rep. 76, 215 (1981)**

**D.I. Blokhintsev, JETP 13, 1295 (1957)**

The inclusive spectra of the secondary hadron $h$ in the central region is determined at high energies by double-Pomeron diagrams.

**V.A. Abramovsky, O.V. Kancheli, and I.D. Mandzhavidze, Sov. J. Nucl. Phys. 13, 630 (1971); Yad. Fiz. 13, 1102 (1971)**

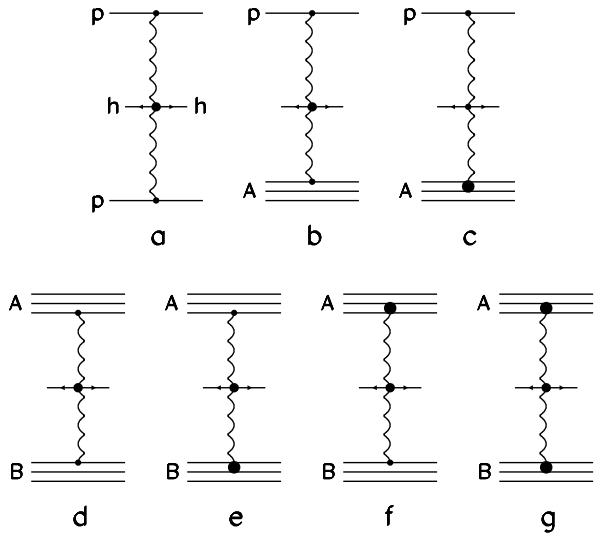


Figure 5: Reggeon diagrams for the different possibilities corresponding to the inclusive spectra of a secondary hadron $h$ produced in the central region in (a) $pp$, (b,c) $p$A, and (d-g) AB collisions. Pomerons are shown by wavy lines.

For nucleus-nucleus collisions there are four possibilities (Figs. 5d, 5e, 5f, and 5g).

The diagram in Fig. 5g corresponds to a new process where a secondary hadron is produced by the interaction of two clusters.

In the case of secondary production from the cluster fragmentation, the inclusive spectra can be calculated in the framework of the QGSM with the same quark and diquark fragmentation functions.

**A.V. Efremov, A.B. Kaidalov, V.T. Kim, G.I. Lykasov, and N.V. Slavin, Sov. J. Nucl. Phys. 47, 868 (1988)**

**A.V. Efremov, A.B. Kaidalov, G.I. Lykasov, and N.V. Slavin, Phys. Atom. Nucl. 57, 874 (1994)**

The only difference comes from the quark and diquark distributions, $u_q^{cl}(x,n,k)$ and $u_{qq}^{cl}(x,n,k)$, where $k$ is the number of nucleons in the cluster.

The distributions $u_i^{cl}(x,n,k)$ can also be calculated by using the Reggeon counting rules, and they take the form:

$$\begin{aligned}
u_{uu}^{cl}(x,n) &= C_{uu}\cdot x^{\alpha_R-2\alpha_B+1}\cdot(k-x)^{-\alpha_R N+m_1}\\
u_{ud}^{cl}(x,n) &= C_{ud}\cdot x^{\alpha_R-2\alpha_B}\cdot(k-x)^{-\alpha_R+N+m_2}\\
u_{u}^{cl}(x,n,k) &= C_{u}\cdot x^{-\alpha_R}\cdot(k-x)^{\alpha_R-2\alpha_B+N+m_2}\\
u_{d}^{cl}(x,n) &= C_{d}\cdot x^{-\alpha_R}\cdot(k-x)^{\alpha_R-2\alpha_B+1+N+m_1}\\
u_{s}^{cl}(x,n) &= C_{d}\cdot x^{-\alpha_R}\cdot(1-x)^{\alpha_R-2\alpha_B+(n-1)+d}\ ,
\end{aligned}$$

where

$$N=2\cdot(1-\alpha_B)\cdot(k-1)\ .$$

The function $u_s^{cl}(x,n)$ does not depend on $k$.

All these functions $u_i^{cl}(x,n,k)$ are normalized to unity.

This approach was succesfully used for the description of cumulative particles produced in $hA$ collisions.

**A.V. Efremov, A.B. Kaidalov, V.T. Kim, G.I. Lykasov, N.V. Slavin, Sov. J. Nucl. Phys. 47, 8568 (1988)**

**A.V. Efremov, A.B. Kaidalov, G.I. Lykasov, N.V. Slavin, Phys. Atom. Nucl. 57, 874 (1994)**

Now we use this approach for describing the enhancement of strangeness production on nuclear targets in the central region.

The probability to find a proton in the backward hemisphere in high energy $pA$ collisions reach values up to 10%.

In the numerical calculations and for every hadron-nucleon interaction we take the probability to interact with a cluster $V^{cl}$, and the probability to actually interact with a nucleon $1 - V^{cl}$.

We use the numerical values:

$$V^{cl} = 0.2 \text{ (for mediumA)} \, , V^{cl} = 0.3 \text{ (for heavy A)} \, ,$$

as the maximal reasonable values of $V^{cl}$.

The QGSM gives a reasonable description of the inclusive spectra of different secondaries produced both in hadron-nucleus and in nucleus-nucleus collisions at energies $\sqrt{s_{NN}} = 14-30$ GeV.

**C. Merino, C. Pajares, and Yu.M. Shabelski, Eur. Phys. J. C71, 1652 (2011)**

**A.B. Kaidalov, K.A. Ter-Martirosyan, and Yu.M. Shabelski, Yad. Fiz. 43, 1282 (1986)**

**J. Dias de Deus and Yu.M. Shabelski, Yad. Fiz. 71, 191 (2008)**

**Yu.M. Shabelski, Sov. J. Nucl. Phys. 45, 143 (1987); Z. Phys. C38, 569 (1988)**

# Inelastic Screening (Percolation Effects)

At RHIC energies the situation drastically changes.

The spectra of secondaries produced in $pp$ collisions are described rather well, but the RHIC experimental data for Au+Au collisions

**B.B. Back et al., PHOBOS Collaboration, Phys. Rev. Lett. 85, 3100 (2000)**

**K. Adcox et al., PHENIX Collaboration, Phys. Rev. Lett. 86, 500 (2001)**

give clear evidence of the inclusive density suppression effects which reduce by a factor $\sim$0.5 the midrapidity inclusive density, when compared to the predictions based on the superposition picture.

**A. Capella, C. Merino, and J. Tran Thanh Van, Phys. Lett. B265 (1991) 415**

This reduction can be explained by the inelastic screening corrections connected to multipomeron interactions

**A. Capella, A. Kaidalov, and J. Tran Thanh Van, Heavy Ion Phys. 9, 169 (1999)**

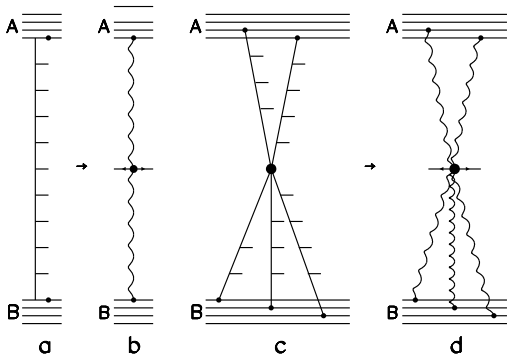


Figure 6: (a) Multiperipheral ladder corresponding to the inclusive cross section of diagram (b), and (c) fusion of several ladders corresponding to the inclusive cross section of diagram (d).

At energies $\sqrt{s_{NN}} \leq 30{-}40$ GeV, the inelastic processes are determined by the production of one (Fig. 6a) or several (Fig. 6c) multiperipheral ladders, and the corresponding inclusive cross sections are described by the diagrams of Fig. 6b and Fig. 6d.

In accordance with the Parton Model, the fusion of multiperipheral ladders shown in Fig. 6c becomes more and more important with the increase of the energy, resulting in the reduction of the inclusive density of secondaries.

**O.V. Kancheli, JETP Lett. 18, 274 (1973)**
**G.V. Davidenko and N.N. Nikolaev, Yad. Fiz. 24, 772 (1976)**

Such processes correspond to the enhancement Reggeon diagrams of the type of Fig. 6d, and to even more complicated ones.

All these diagrams are proportional to the squared longitudinal form factors of both colliding nuclei, so their contribution becomes negligible when the energy decreases.

The RHIC energies are just of the order of magnitude needed to observe this effect.

**A. Capella, A. Kaidalov, and J. Tran Thanh Van, Heavy Ion Phys. 9, 169 (1999)**

Unfortunately, all quantitative estimations are model dependent, and though in some models the number of unknown parameters can be reduced, the uncertainties remain significant.

Another possibility to estimate the contribution of the diagrams with Pomeron interaction comes from Percolation Theory.

**J. Dias de Deus, R. Ugoccioni, and A. Rodrigues, Phys. Lett. B458, 402 (1999)**

**M.A. Braun and C. Pajares, Phys. Rev. Lett. 85, 4864 (2000)**

**J. Dias de Deus and Yu.M. Shabelski, Eur. Phys. J. A20, 457 (2004)**

The percolation approach and its previous version, the String Fusion Model

**C. Merino, C. Pajares, and J. Ranft, Phys. Lett. B276, 168 (1992)**

**H.J. Möhring, J. Ranft, C. Merino, and C. Pajares, Phys. Rev. D47, 4142 (1993).**

**N.S. Amelin, M.A. Braun, and C. Pajares, Z. Phys. C63, 507 (1994)**

predicted the multiplicity suppression seen at RHIC energies, long before any RHIC data were measured.

Calculations of inclusive densities and multiplicities in percolation theory both in $pp$, and in heavy ion collisions, are in good agreement with the experimental data in a wide energy region.

**I. Bautista, J. Dias de Deus, G. Milhano, and C. Pajares, Phys. Lett. B715, 230 (2012)**

To account for the percolation effects in the QGSM, it is technically more simple to consider the maximal number of Pomerons $n_{max}$ emitted by one nucleon in the central region that can be cut.

**C. Merino, C. Pajares, and Yu.M. Shabelski, Eur. Phys. J. C59, 691 (2009). and arXiv:0802.2195 [hep-ph]**

These cut Pomerons lead to the different final states.

Then the contributions of all diagrams with $n \leq n_{max}$ are accounted for as at lower energies.

The larger number of Pomerons $n > n_{max}$ can also be emitted obeying the unitarity constraint, but due to the fusion in the final state (at the quark-gluon string stage), the cut of $n > n_{max}$ Pomerons results in the same final state as the cut of $n_{max}$ Pomerons.

By doing this, all model calculations become very similar to the percolation approach.

The QGSM fragmentation formalism allows one to calculate the integrated over $p_T$ spectra of different secondaries as the functions of rapidity and $x_F$.

We obtain a reasonable agreement with the experimental data on the inclusive spectra of secondaries produced in d+Au collisions at RHIC energy with a value $n_{max} = 13$

**C. Merino, C. Pajares, and Yu.M. Shabelski, Eur. Phys. J. C59, 691 (2009). and arXiv:0802.2195 [hep-ph]**

and in p+Pb collisions at LHC energy with the value $n_{max} = 23$.

**C. Merino, C. Pajares, and Yu.M. Shabelski, arXiv:1207.6900[hep-ph]**

The number of strings that can be used for the secondary production should increase with the initial energy.

**J. Dias de Deus and C. Pajares, Phys. Lett. B695, 211 (2012) and arXiv:1011.1099[hep-ph]**

# NUMERICAL RESULTS

## Net Baryon Spectra

QGSM description of the $x_F$-spectra of secondary protons and antiprotons measured by the NA49 Collaboration in $pp$ collisions at 158 GeV/c.

**T. Anticic et al., NA49 Collaboration, arXiv:1004.1889[hep-ex]**

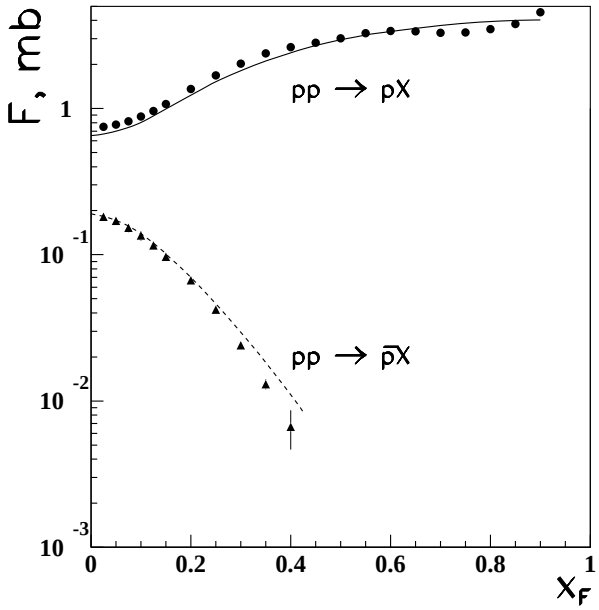


Figure 7: QGSM $x_F$-spectra of secondary protons and antiprotons produced in $pp$ collisions at 158 GeV/c compared to the experimental data by the NA49 Collaboration.

The QGSM results for net proton ($p - \bar{p}$) and net $\Lambda$-hyperon ($\Lambda - \bar{\Lambda}$) productions at 200 GeV per nucleon are also compared to the experimental data by the NA35 Collaboration

**T. Alber et al., NA35 Collaboration, Eur. Phys. J. C2, 643 (2008) and arXiv: 9711001[hep-ex]**

We present the data for net baryon production by proton beam interaction with $^{32}$S and $^{197}$Au nuclear targets in the central and beam fragmentation regions as function of rapidity in the laboratory system.

The absolute normalization of $dn/dy$ in all cases is determined by the data of proton and antiproton production in $pp$ collisions at similar energies.

The corrections for very high energy interactions are negligible at this energy.

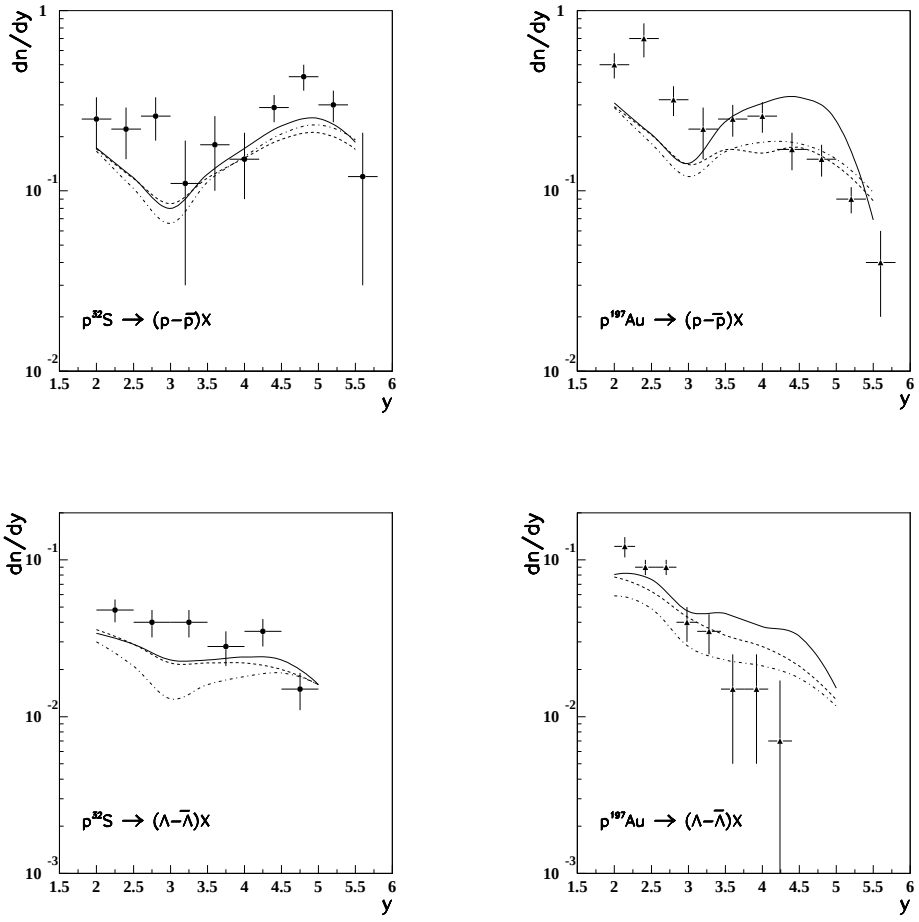


Figure 8: Net proton $p - \bar{p}$ (upper panels) and net $\Lambda$-hyperon $\Lambda - \bar{\Lambda}$ (lower panels) production in $p-^{32}$S (left panels) and $p-^{197}$Au (right panels) collisions at 200 GeV per nucleon. Solid curves show the QGSM calculations with both SJ and cluster contributions, dashed curves with SJ contributions but without the cluster contributions, and dotted curves without both SJ and cluster contributions.

In the case of net proton production in $p-^{32}$S collisions, all three curves are close to each other and they are in reasonable agreement with the experimental data.

In the case of $p-^{197}$Au collisions the number of net protons is too small at small rapidities, what can be explained by the influence of the target fragmentation region.

The nuclear cluster contribution, which is important mainly in the beam fragmentation region, seems to be too large.

In the case of net $\Lambda$-hyperon production the experimental error bars are rather large, and one can talk of general semiquantitative agreement of the QGSM calculations with the experimental data.

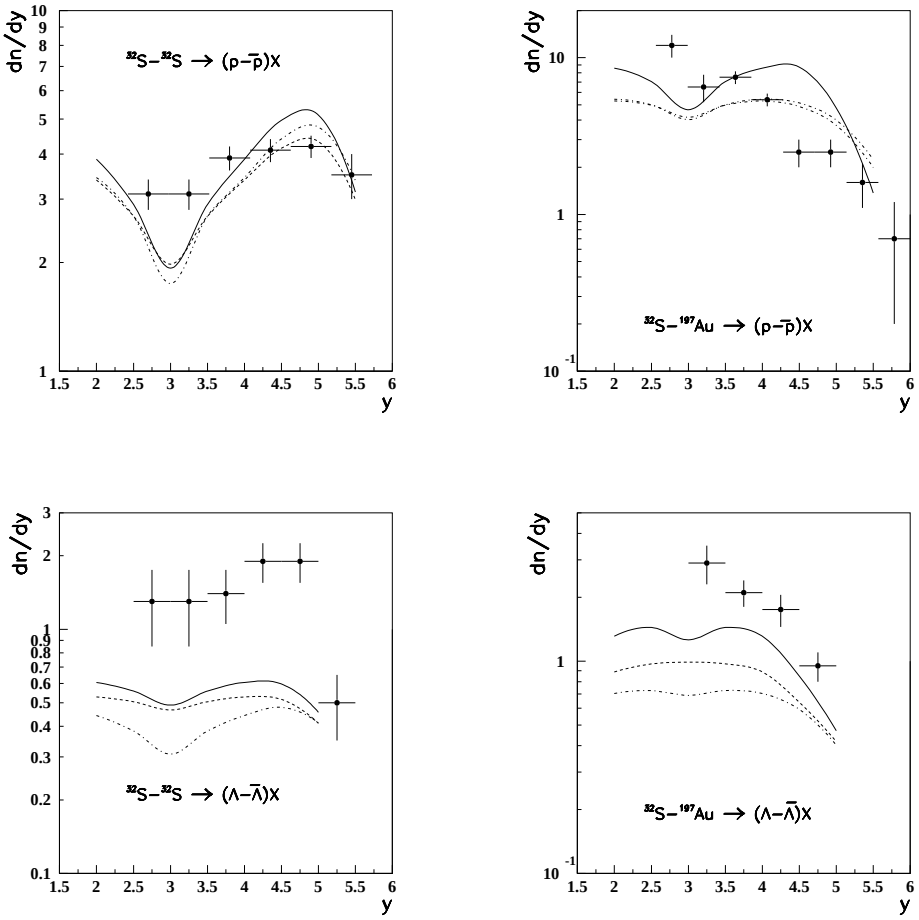


Figure 9: Net proton $p - \bar{p}$ (upper panels) and net $\Lambda$-hyperon $\Lambda - \bar{\Lambda}$ (lower panels) production in $^{32}$S - $^{32}$S (left panels) and in $^{32}$S - $^{197}$Au (right panels) collisions at 200 GeV per nucleon. Solid curves show the QGSM calculations with both SJ and cluster contributions, dashed curves with SJ contributions but without the cluster contributions, and dotted curves without both SJ and cluster contributions.

For the sulphur $^{32}$S beam, the theoretical calculations are in reasonable agreement with the data for net proton production, whereas the data on net $\Lambda$-hyperon production are systematicaly higher than all calculated curves.

In any case, though, all disagreements are not large than $\sim$30%.

The data of the NA35 Collaboration

**T. Alber et al., NA35 Collaboration, Eur. Phys. J. C2, 643 (2008) and arXiv: 9711001[hep-ex]**

are compatible with the results of the NA44 Collaboration

**G. Bearden et al., NA44 Collaboration, Phys. Rev. C57, 837 (19988) and arXiv:9711004[nucl-ex]**

# $\Lambda$ and $\bar{\Lambda}$ Production in Midrapidity Region

We compare the QGMS results to the experimental data by the NA49 Collaboration

**T. Anticic et al., NA49 Collaboration, Phys. Rev. C80, 034906 (2009) and arXiv:0906.0469[nucl-ex]**

for yields of $\Lambda$ and $\bar{\Lambda}$ hyperons in midrapidity region ($|y| < 0.4$) in the central C+C, Si+Si, and Pb+Pb collisions (5% centrality), at 158 GeV per nucleon.

We also present the data obtained by the NA57 Collaboration

**F. Antinori et al., NA57 Collaboration, J. Phys. G32, 427 (2006) and arXiv:0601021[nucl-ex]**

for $\Lambda$ and $\bar{\Lambda}$ yields in midrapidity region $|y| < 0.5$ in the minimum bias $p$+Be and $p$+Pb interactions, and in central (5% centrality) Pb+Pb collisions at 158 GeV per nucleon.

Unfortunately, the data by the NA49 and NA57 collaborations are not compatible.

Hyperon production at higher energies in midrapidity region was also measured at RHIC. The data by the STAR Collaboration

**M.M. Aggarwal et al., STAR Collaboration, Phys. Rev. C83, 024901 (2011) and arXiv:1010.0142[nucl-ex]**

**G. Agakishiev et al., STAR Collaboration, Phys. Rev. Lett. 108, 072301 (2012) and arXiv:1107.2955[nucl-ex]**

for Au + Au and Cu + Cu collisions at $\sqrt{s_{NN}} = 62.4$ GeV and 200 Gev are also compared to the QGSM predictions for central Pb+Pb collisions at the LHC energy $\sqrt{s_{NN}} = 3$ TeV.

In Table 1 we present the numerical values of the experimental NA49, NA57, and STAR data for $\Lambda$ and $\bar{\Lambda}$ production at 158GeV per nucleon, and at STAR energies, and the corresponding description by the QGSM.

| $\sqrt{s}$ | Reaction | QGSM | Experiment dn/dy |
|---|---|---|---|
| 17.2 | C+C$\to\Lambda$ | 0.237 | $0.24 \pm 0.01 \pm 0.04$ |
| | C+C$\to\bar{\Lambda}$ | 0.064 | $0.064 \pm 0.003 \pm 0.010$ |
| 17.2 | Si+Si$\to\Lambda$ | 0.69 | $0.68 \pm 0.04 \pm 0.13$ |
| | Si+Si$\to\bar{\Lambda}$ | 0.17 | $0.16 \pm 0.007 \pm 0.038$ |
| 17.2 | Pb+Pb$\to\Lambda$ | 9.4 | $12.9 \pm 0.7 \pm 1.5$ |
| | Pb+Pb$\to\bar{\Lambda}$ | 2.05 | $1.4 \pm 0.3 \pm 0.2$ |
| 17.2 | p+Be$\to\Lambda$ | 0.034 | $0.034 \pm 0.0005 \pm 0.003$ |
| (mb) | p+Be$\to\bar{\Lambda}$ | 0.010 | $0.011 \pm 0.0002 \pm 0.001$ |
| 17.2 | p+Pb$\to\Lambda$ | 0.074 | $0.060 \pm 0.002 \pm 0.006$ |
| (mb) | p+Pb$\to\bar{\Lambda}$ | 0.0019 | $0.015 \pm 0.001 \pm 0.002$ |
| 17.2 | Pb+Pb$\to\Lambda$ | 9.4 | $18.5 \pm 1.1 \pm 1.8$ |
| | Pb+Pb$\to\bar{\Lambda}$ | 2.05 | $2.44 \pm 0.14 \pm 0.24$ |
| 62.4 | Au+Au$\to\Lambda$ | 11.1 | $15.7 \pm 0.3 \pm 2.3$ |
| | Au+Au$\to\bar{\Lambda}$ | 8.2 | $8.3 \pm 0.2 \pm 1.1$ |
| 200 | Cu+Cu$\to\Lambda$ | 3.82 | $4.68 \pm 0.45$ |
| | Cu+Cu$\to\bar{\Lambda}$ | 3.34 | $3.79 \pm 0.37$ |
| 200 | Au+Au$\to\Lambda$ | 14.2 | $14.8 \pm 2.4$ |
| | Au+Au$\to\bar{\Lambda}$ | 12.1 | $11.7 \pm 0.9$ |
| 3000 | Pb+Pb$\to\Lambda$ | 36.2 | – |
| | Pb+Pb$\to\bar{\Lambda}$ | 35.6 | – |

Table 1 ($\sqrt{s}$ in GeV)

# Conclusions

- The QGSM provides a reasonable description of nucleon and $\Lambda$, as well as of their antiparticles, production in nucleon-nucleus and nucleus-nucleus collisions at high energies.
- The level of numerical accuracy is of about 20−30%.
- Part of the uncertainty is connected to discrepancies among the different experimental data.
- Inclusive densities of $\overline{\Xi}^+$ hyperons are reasonably reproduced for the cases of p+Be and p+Pb collisions.
- Inclusive densities of $\overline{\Xi}^+$ hyperons are several times underestimated in the case of central Pb+Pb interactions.
- For $\overline{\Omega}^+$ production in central Pb+Pb collisions the disagreement is larger than one order of magnitude.
- The physical reasons for these observed disagreements will be discussed in a separate paper now in progress.

# TRIBUTE TO A.B. KAIDALOV

- The authors (GHA,CM,YMSh) want to pay tribute to A.B Kaidalov, and to acknowledge his enlightening comments during the preparation work for this paper, from his privileged position among the first, with his colleagues from DUBNA (AVE,GIL,NVS), to consider cluster interactions in the frame of string models.